NACA

RESEARCH MEMORANDUM

WIND-TUNNEL INVESTIGATION OF THE DAMPING IN ROLL OF THE BELL X-1A RESEARCH AIRPLANE AND ITS COMPONENTS AT SUPERSONIC SPEEDS

By Russell W. McDearmon and Frank L. Clark

Langley Aeronautical Laboratory
Langley Field, Va.

NATIONAL ADVISORY COMMITTEE
FOR AERONAUTICS

WASHINGTON

January 10, 1956

NATIONAL ADVISORY COMMITTEE FOR AERONAUTICS

RESEARCH MEMORANDUM

WIND-TUNNEL INVESTIGATION OF THE DAMPING IN ROLL OF THE BELL X-1A RESEARCH AIRPLANE AND ITS COMPONENTS AT SUPERSONIC SPEEDS

By Russell W. McDearmon and Frank L. Clark

SUMMARY

Experimental values of the damping in roll of the Bell X-1A research airplane and its components have been obtained at Mach numbers of 1.62, 1.94, 2.22, 2.41, and 2.62, at zero angle of attack. Severe losses in the damping in roll C_{l_p} were obtained near a Mach number of 2.22 for the complete model and the configuration with body, wing, and vertical tail. For the complete model this loss was largely alleviated by removing the dorsal and ventral fins.

The wing was the predominant contributor to the damping in roll throughout the Mach number range, although the contributions of the other airplane components to the damping in roll were significant in the Mach number region from 2.22 to 2.41.

In general, the damping in roll C_{l_p} of the complete model and for the model with body, wing, and vertical tail was predicted adequately by theory, except in the Mach number region from 2.22 to 2.41, where component interference effects caused large deviations from theory. The damping in roll C_{l_p} of the body-wing model was predicted adequately by theory throughout the Mach number range of the tests.

INTRODUCTION

The X-1A research airplane has exhibited unsatisfactory handling qualities in recent flight tests at supersonic speeds. In order to obtain some experimental information to provide insight into the causes of these unsatisfactory handling qualities, a general program of investigations is being undertaken in the Langley 9-inch supersonic tunnel of some of the dynamic and static stability characteristics of the X-1A.

One of the more important stability derivatives which must be evaluated in order to predict the dynamic stability characteristics of a given airplane configuration is the damping in roll C_{l_p}.

Considerable theoretical work has been done to predict C_{l_p} at supersonic speeds for isolated wings (e.g., see refs. 1 and 2), certain restricted wing-body combinations, cruciform wings, slender tail configurations (e.g., see refs. 3 to 6), and a typical airplane configuration (see ref. 7). The experimental information available at supersonic speeds includes the results of wind-tunnel investigations of C_{l_p} for a large class of wing plan forms (see refs. 8 and 9), free-flight investigations of C_{l_p} for various wing-body and missile configurations, such as those reported in references 10 and 11, and investigations utilizing other techniques, such as those reported in reference 12. The present investigation provides some experimental values of C_{l_p} for a particular airplane configuration and extends the knowledge of the component effects on C_{l_p} for complete airplane configurations at supersonic speeds.

In the present investigation, C_{l_p} for the X-1A research airplane and its components was obtained at Mach numbers of 1.62, 1.94, 2.22, 2.41, and 2.62, at zero angle of attack. The test Reynolds number range for the complete configuration was from 0.24×10^6 to 0.44×10^6, based on the mean aerodynamic chord of the wing. However, all tests were conducted with transition strips on the components in order to simulate more closely the boundary-layer conditions encountered at higher Reynolds numbers. The primary purpose of this investigation was to determine the damping in roll of the complete configuration and the contributions of the components to the damping in roll. Included were determinations of the effects of the dorsal and ventral fins on C_{l_p} for the complete configuration. In this report, the term "dorsal fin" includes the canopy and the conduit which extends from the canopy rearward, and is faired smoothly into the vertical tail. The term "ventral fin" refers to the smaller conduit which traverses a major part of the ventral portion of the body. Comparisons were made with some theoretical predictions.

SYMBOLS

b	wing span, ft
C_l	rolling-moment coefficient, $\frac{L}{qSb}$

[redacted]

C_{l_p} damping-in-roll derivative, $\frac{\partial C_l}{\partial \frac{pb}{2V}}$

Γ circulation at any spanwise station along the wing, ft^2/sec

L rolling moment, ft-lb

M free-stream Mach number

p rolling angular velocity, radians/sec

$\frac{pb}{2V}$ wing-tip helix angle, radians

q free-stream dynamic pressure, lb/sq ft

r radial distance from center of vortex, ft

S total wing area, including portion submerged in body, sq ft

V free-stream velocity, ft/sec

v tangential velocity at a distance r from center of vortex, $\frac{\Gamma_{max}}{2\pi r}$, ft/sec

Subscripts and configuration identification:

max maximum

BW body and wing

BV body and vertical tail

BVH body, vertical tail, and horizontal tail

BWV body, wing, and vertical tail

BWVH body, wing, vertical tail, and horizontal tail

[redacted]

APPARATUS

Wind Tunnel

All tests were conducted in the Langley 9-inch supersonic tunnel, which is a closed-circuit, continuous-operation type in which the stream pressure, temperature, and humidity can be controlled at all times during tunnel operation. Different test Mach numbers are provided by interchangeable nozzle blocks which form test sections approximately 9 inches square. Eleven fine-mesh turbulence-damping screens are installed in the settling chamber ahead of the supersonic nozzle. The turbulence level of the tunnel is considered low, based on past turbulence-level measurements. A schlieren optical system is provided for qualitative flow observation.

Models, Support, and Rolling-Moment Balance

A drawing of the complete 1/62-scale model of the X-1A is presented in figure 1. The sting was an integral part of the model body. In order to use a sting of sufficient strength to withstand the forces which would be encountered in testing, it was necessary to alter the shape of the aft portion of the body, as shown in figure 1. The effect of this alteration on C_{l_p} was believed to be negligible.

Three identical bodies were constructed, one for the BWV and BWVH configurations, one for the BW configuration, and one for the BV and BVH configurations. The wing and tail units were removable, so that either could be installed on the desired body. The nose portions of the bodies were made of aluminum. The remaining portions of the bodies and the integral stings and the wing were made of steel. The tail surfaces and the dorsal and ventral fins were molded from plastic materials. This arrangement of model parts and selection of materials resulted primarily from the necessity for accurately mass-balancing the models.

Since the tail surfaces were molded from plastic materials, they may have experienced slight bending or twisting when tested. However, the resulting aeroelastic effect on the contributions of the tail surfaces to C_{l_p} is believed to have been small.

The BWVH configuration was tested with the dorsal fin removed, and with the dorsal and ventral fins removed. When the dorsal fin was removed, the vertical tail was faired smoothly into the body as shown in figure 1. When the dorsal and ventral fins were removed, the body became a body of revolution.

[redacted]

All models were tested with finely pulverized salt transition strips on the components. The transition strips were located as shown in figure 1 to create a turbulent boundary layer over most of the model and thereby more closely simulate full-scale conditions. The effectiveness of similar transition strips in creating a turbulent boundary layer may be seen in reference 13.

Photographs of the damping-in-roll test apparatus are presented in figure 2. The model sting was inserted into the spindle of the rolling-moment balance and secured by a Woodruff key and setscrews. The spindle was rotated by means of gears and an electric motor outside the tunnel. The rolling velocity was measured with a Stroboconn frequency indicator which was modified to indicate revolutions per minute by means of a generator attached to the rear of the spindle. The rolling moments were measured by strain gages on the spindle and were transmitted through slip rings and brushes to a Brown strain indicator unit outside the tunnel.

PRECISION

The precision of the data has been determined by estimating the accuracies of the measured quantities and evaluating their effects on the coefficient C_l and the parameter $pb/2V$. The probable error in the strain-gage indication produced the following errors in C_l:

M	Error in C_l for configurations -	
	BWVH, BWV, BW	BV, BVH
1.62	±0.00035	±0.00015
1.94	±.00040	±.00015
2.22	±.00045	±.00017
2.41	±.00050	±.00018
2.62	±.00040	±.00020

[redacted]

Error in the measurement of the rolling velocity caused a maximum error in $pb/2V$ of ± 0.00008. The surveyed variation of each of the free-stream Mach numbers is about ± 0.01, which produced a maximum error in $pb/2V$ of ± 0.00003. Thus the maximum total error in $pb/2V$ was ± 0.00011.

Model alinement was maintained to within $\pm 0.1^\circ$ of zero pitch and yaw with respect to the tunnel center line.

The rolling-moment balance was calibrated statically before and at intervals during the testing to ascertain that there were no changes in the strain-gage constant.

Throughout the tests, the moisture content in the tunnel was kept sufficiently low to insure that the effects of condensation were negligible.

RESULTS AND DISCUSSION

The variations of rolling-moment coefficient with wing-tip helix angle for the various configurations are presented in figure 3. It may be seen in figure 3(c) that two different variations of C_l with $pb/2V$ were obtained at $M = 2.22$ for BWVH with the dorsal and ventral fins in place. The term "alternate" employed in this figure signifies that a separate dorsal fin was used on the model in the second test. The "alternate" dorsal fin was cast from the same mold as the original dorsal fin; however, small errors in reproduction and installation on the model may have caused its external contour to differ slightly from that of the original. The differences in the variations of C_l with $pb/2V$ which were obtained in the two tests are believed to have been caused by viscous effects associated with slight differences in the external contour of the dorsal fin.

The Contributions of the Airplane Components to C_{l_p}

The variations with Mach number of C_{l_p} for the complete model and its components are presented in figure 4. The values of C_{l_p} were obtained by taking the slopes of the variations of C_l with $pb/2V$ presented in figure 3.

The most striking feature of the results is the fact that severe losses in C_{l_p} were experienced near $M = 2.22$ by BWVH and BWV with the dorsal and ventral fins in place. It should be noted that neither the minimum values of C_{l_p} in the vicinity of $M = 2.22$ for

the configurations containing the wing nor the Mach numbers at which they occurred were definitely established, although the fairing of the curves of figure 4 indicated that the minimum values probably occurred between $M = 2.22$ and $M = 2.41$. In view of this uncertainity, the curves were dashed in the Mach number range from 1.94 to 2.41. Also, since BWVH with the dorsal and ventral fins in place was tested twice at $M = 2.22$, so that two somewhat different values of C_{l_p} were obtained, the curve for this configuration was faired midway between the two values in figure 4. The value of C_{l_p} shown in figure 4 for BWVH with the "alternate" dorsal fin and ventral fin in place represents the slope of the variation of C_l with $pb/2V$ over a range of $pb/2V$ from 0 to 0.019 or from 0.024 to 0.036 (fig. 3(c)), the slope over a range of $pb/2V$ from 0.019 to 0.024 not being considered.

For BWVH and BWV with the dorsal and ventral fins in place, gradual decreases in C_{l_p} occurred as the Mach number was increased from 1.62 to 1.94. Abrupt decreases in C_{l_p} took place as the Mach number was increased from 1.94 to 2.22. Following the apparent minimum values of C_{l_p} which were obtained near $M = 2.22$, rather rapid increases in C_{l_p} were obtained as the Mach number was increased to $M = 2.41$ and $M = 2.62$, exhibiting a tendency to revert to the trends of the variations of C_{l_p} at $M = 1.62$ and $M = 1.94$. For BW with dorsal and ventral fins in place, no significant reduction in C_{l_p} was obtained near $M = 2.22$. The wing was the predominant contributor to C_{l_p} throughout the Mach number range, although the contributions of the other airplane components to C_{l_p} were significant in the Mach number region from 2.22 to 2.41.

In an attempt to determine the cause of the drastic loss in C_{l_p} experienced by BWVH near $M = 2.22$, the dorsal fin was removed. This resulted in approximately a 35-percent increase in C_{l_p} for BWVH at $M = 2.22$. Next, the ventral fin was removed, and an additional 17-percent increase in C_{l_p} was obtained at $M = 2.22$, giving an overall increase in C_{l_p} of approximately 52 percent at $M = 2.22$ with the dorsal and ventral fins removed. The BWVH configuration with dorsal and ventral fins removed was then tested at the other Mach numbers of the investigation, and at all Mach numbers C_{l_p} for BWVH was somewhat higher with the dorsal and ventral fins removed than with the fins in place.

These results show that the severe loss in C_{l_p} experienced by BWVH near $M = 2.22$, as well as the level of C_{l_p} for BWVH throughout

the Mach number range of the tests, was definitely associated with the interference effects of the dorsal and ventral fins. The fact that with the dorsal and ventral fins in place BW experienced no significant reduction in C_{l_p} whereas BWVH and BWV experienced sizeable losses in C_{l_p} near $M = 2.22$ indicates that the losses resulted primarily from the effects of the dorsal and ventral fins on the tail panels. The remaining slight reduction in C_{l_p} which was obtained near $M = 2.22$ for BWVH with the dorsal and ventral fins removed can only be attributed to some combination of body-wing-tail interference effects.

Some schlieren photographs of the flow about the complete model at zero rolling velocity are presented in figure 5. These photographs show the positions with respect to the wing of the strong shock waves from the body nose and the blunt nose (or canopy portion) of the dorsal fin as well as the weaker shock wave from the nose of the ventral fin. Also apparent at $M = 2.41$ is an extraneous shock wave which is caused by a slight imperfection in one of the nozzle blocks. As may be readily confirmed, this shock is inclined at an angle of less than 1° with respect to the Mach angle and is, therefore, obviously weak. Past stream surveys have shown no significant effect of this shock wave, and it does not strike the model. Thus, its influence on C_{l_p} was negligible.

As shown in figure 4, a reasonable level of C_{l_p} was obtained for BV at all Mach numbers except $M = 2.41$, where C_{l_p} was nearly zero. However, the almost complete lack of C_{l_p} obtained for BVH throughout the Mach number range was somewhat surprising. This may have been caused by interference between the vertical tail and the horizontal tail, or the effects of the dorsal and ventral fins on the tail.

Comparisons of the Experimental Values of C_{l_p} with Some Theoretical Predictions

The variations with Mach number of the experimental and theoretical C_{l_p} of the various configurations are presented in figure 6. The theoretical predictions of C_{l_p} for BW were obtained from reference 1 for an isolated thin wing with the same plan form as the wing of the X-1A. The effect of the body on C_{l_p} was neglected.

The theoretical predictions of C_{l_p} for BV were obtained by taking one-half of the values given in reference 1 for a wing containing two panels, each of which had approximately the same plan form as the vertical tail. The theoretical predictions of C_{l_p} for BVH consisted of

the values of C_{l_p} for the vertical tail plus the values of C_{l_p} for the horizontal tail. The theoretical values of C_{l_p} for the horizontal tail were obtained from reference 1. Obviously, the predictions of C_{l_p} for the horizontal tail were not exactly applicable to the present case, since the wings of reference 1 were assumed to roll about the root chords, whereas the horizontal tail of the X-1A model was located some distance above the body axis, and hence was not rolling about its root chord. However, these were the only theoretical predictions available, and they are believed to be fair approximations of C_{l_p}, assuming no interference. For BV and BVH the effect of the body on C_{l_p} was neglected.

The theoretical predictions of C_{l_p} for BWV and BWVH represent the net contributions of the wing and tail panels to C_{l_p}, obtained as described above, plus approximations of the effects of the wing flow field on the tail panels. The approximations consisted of representing the wake behind the wing by four infinite line vortices, determining graphically the sidewash and upwash (or downwash) velocities induced on the vertical tail and horizontal tail, respectively, by the vortices, and calculating the resulting rolling moments on the tail panels.

The employment of more exact methods of estimating the effects of the wing flow field including body effects was considered too involved for the purposes of this paper.

The spanwise circulation distribution for the rolling wing was obtained from reference 14, and is illustrated in figure 7(a). The continuous circulation distribution was replaced by a step function, as shown in figure 7(a), representing the four line vortices originating at the trailing edge. The strength of each vortex was proportional to the height of its step (i.e., proportional to Γ_{max}). The spanwise location of the inboard vortex was determined by making the area under the stepped curve equal to the area under the circulation curve, over those portions of the curves from the roll axis to the spanwise location of Γ_{max}. The spanwise location of the outboard vortex was determined by making the area under the stepped curve equal to the area under the circulation curve, over those portions of the curves from the spanwise location of Γ_{max} to the wing tip.

The line vortices were assumed to originate at the wing trailing edge and travel straight back, permitting the vortices in the vicinity of the tail to be depicted as shown in figure 7(b). At each of several spanwise locations along the vertical tail, the sidewash component of the resultant velocity due to the four vortices was determined. At each of several spanwise locations along the horizontal tail, the upwash

(or downwash) component of the resultant velocity due to the four vortices was determined. This was accomplished at each spanwise location by calculating the tangential velocity v at any radial distance r from the center of the vortex from the incompressible relation

$$v = \frac{\Gamma_{max}}{2\pi r}$$

for each vortex (the variation of v with r is given in figure 7(b)), representing the values of v by vectors, and obtaining the sidewash or downwash component of the resultant velocity vector.

The rolling moments induced on the tail panels by the sidewash and downwash velocities were calculated by use of the method of reference 15.

Figures 6(a) and 6(b) show that, in general, C_{l_p} for BWVH and BWV was predicted adequately by theory, except in the Mach number region from $M = 2.22$ to 2.41, where component interference effects caused large deviations from theory. For BW, good agreement between the experimental and theoretical C_{l_p} was obtained throughout the Mach number range of the tests. Figure 6(c) shows that the experimental C_{l_p} for BV was in fair agreement with theory at all Mach numbers except 2.41, and C_{l_p} for BVH was overestimated by theory throughout the Mach number range.

CONCLUSIONS

Wind-tunnel investigations of the damping in roll C_{l_p} of the Bell X-1A research airplane and its components were made at Mach numbers of 1.62, 1.94, 2.22, 2.41, and 2.62, at zero angle of attack. From the results of these investigations the following conclusions are indicated:

1. A severe loss in the damping in roll C_{l_p} was experienced by the complete model near a Mach number of 2.22. Similar results were obtained for the configuration with body, wing, and vertical tail.

2. The loss in C_{l_p} experienced by the complete model near a Mach number of 2.22 was largely alleviated by removing the dorsal and ventral fins. The phenomena near a Mach number of 2.22 resulted primarily from the effects of the dorsal and ventral fins on the tail panels.

[redacted]

3. The wing was the predominant contributor to the damping in roll C_{l_p} throughout the Mach number range, although the contributions of the other airplane components to C_{l_p} were significant in the Mach number region from 2.22 to 2.41.

4. In general, the damping in roll C_{l_p} of the complete model and of the configuration with body, wing, and vertical tail was predicted adequately by theory, except in the Mach number region from 2.22 to 2.41, where component interference caused large deviations from theory. The damping in roll C_{l_p} of the body-wing model was predicted adequately by theory throughout the Mach number range of the tests.

Langley Aeronautical Laboratory,
National Advisory Committee for Aeronautics,
Langley Field, Va., August 31, 1955.

[redacted]

REFERENCES

1. Harmon, Sidney M., and Jeffreys, Isabella: Theoretical Lift and Damping in Roll of Thin Wings With Arbitrary Sweep and Taper at Supersonic Speeds - Supersonic Leading and Trailing Edges. NACA TN 2114, 1950.

2. Malvestuto, Frank S., Jr., Margolis, Kenneth, and Ribner, Herbert S.: Theoretical Lift and Damping in Roll at Supersonic Speeds of Thin Sweptback Tapered Wings With Streamwise Tips, Subsonic Leading Edges, and Supersonic Trailing Edges. NACA Rep. 970, 1950. (Supersedes NACA TN 1860.)

3. Lomax, Harvard, and Heaslet, Max. A.: Damping-In-Roll Calculations for Slender Swept-Back Wings and Slender Wing-Body Combinations. NACA TN 1950, 1949.

4. Miles, John W.: On the Damping in Roll of a Slender Cruciform Winged Body. NAVORD Rep. 2043 (NOTS 732), U. S. Naval Ord. Test Station (Inyokern, Calif.), July 16, 1953.

5. Ribner, Herbert S.: Damping In Roll of Cruciform and Some Related Delta Wings at Supersonic Speeds. NACA TN 2285, 1951.

6. Bobbitt, Percy J., and Malvestuto, Frank S., Jr.: Estimation of Forces and Moments Due to Rolling for Several Slender-Tail Configurations at Supersonic Speeds. NACA TN 2955, 1953.

7. Margolis, Kenneth, and Bobbitt, Percy J.: Theoretical Calculations of the Stability Derivatives at Supersonic Speeds for a High-Speed Airplane Configuration. NACA RM L53G17, 1953.

8. Brown, Clinton E., and Heinke, Harry S., Jr.: Preliminary Wind-Tunnel Tests of Triangular and Rectangular Wings in Steady Roll at Mach Numbers of 1.62 and 1.92. NACA RM L8L30, 1949.

9. McDearmon, Russell W., and Heinke, Harry S., Jr.: Investigations of the Damping in Roll of Swept and Tapered Wings at Supersonic Speeds. NACA RM L53A13, 1953.

10. Bland, William M., Jr., and Sandahl, Carl A.: A Technique Utilizing Rocket-Propelled Test Vehicles for the Measurement of the Damping in Roll of Sting-Mounted Models and Some Initial Results for Delta and Unswept Tapered Wings. NACA TN 3314, 1955. (Supersedes NACA RM L50D24.)

11. Hopko, Russell N.: A Flight Investigation of the Damping in Roll and Rolling Effectiveness Including Aeroelastic Effects of Rocket-Propelled Missile Models Having Cruciform, Triangular, Interdigitated Wings and Tails. NACA RM L51D16, 1951.

12. Boissevain, Alfred G.: Experimental Investigation of the Damping In Roll of Cruciform Triangular Wing-Body Combinations at Mach Numbers From 1.5 to 6.0. NACA RM A54B15a, 1954.

13. Fallis, William B.: On Distributed Roughness as a Means of Fixing Transition at High Supersonic Speeds. Jour. Aero. Sci., (Readers' Forum), vol. 22, no. 5, May 1955, p. 339.

14. Martin, John C., and Jeffreys, Isabella: Span Load Distributions Resulting From Angle of Attack, Rolling, and Pitching for Tapered Sweptback Wings With Streamwise Tips - Supersonic Leading and Trailing Edges. NACA TN 2643, 1952.

15. Alden, Henry L., and Schindel, Leon H.: The Lift, Rolling Moment, and Pitching Moment on Wings in Nonuniform Supersonic Flow. Jour. Aero. Sci., vol. 19, no. 1, Jan. 1952, pp. 7-14.

[redacted]

Wing.	
Area	4.864 sq in.
Span	5.420 in.
Aspect ratio	6
Section	65_1-008 (a=1)
Root incidence	2.5°
Tip incidence	1.5°
Horizontal tail:	
Area	0.974 sq in.
Section	65-006
Vertical tail:	
Area	0.958 sq in.
Section	65-008

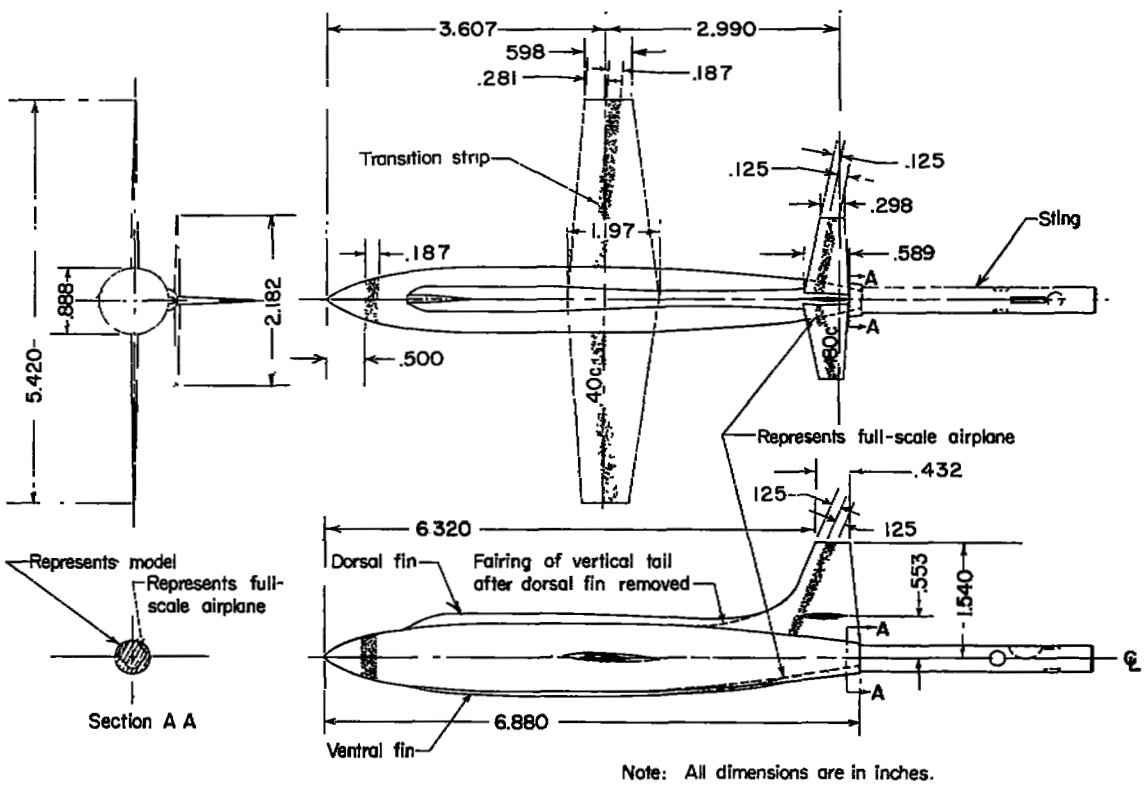

Figure 1.- Drawing of the complete model.

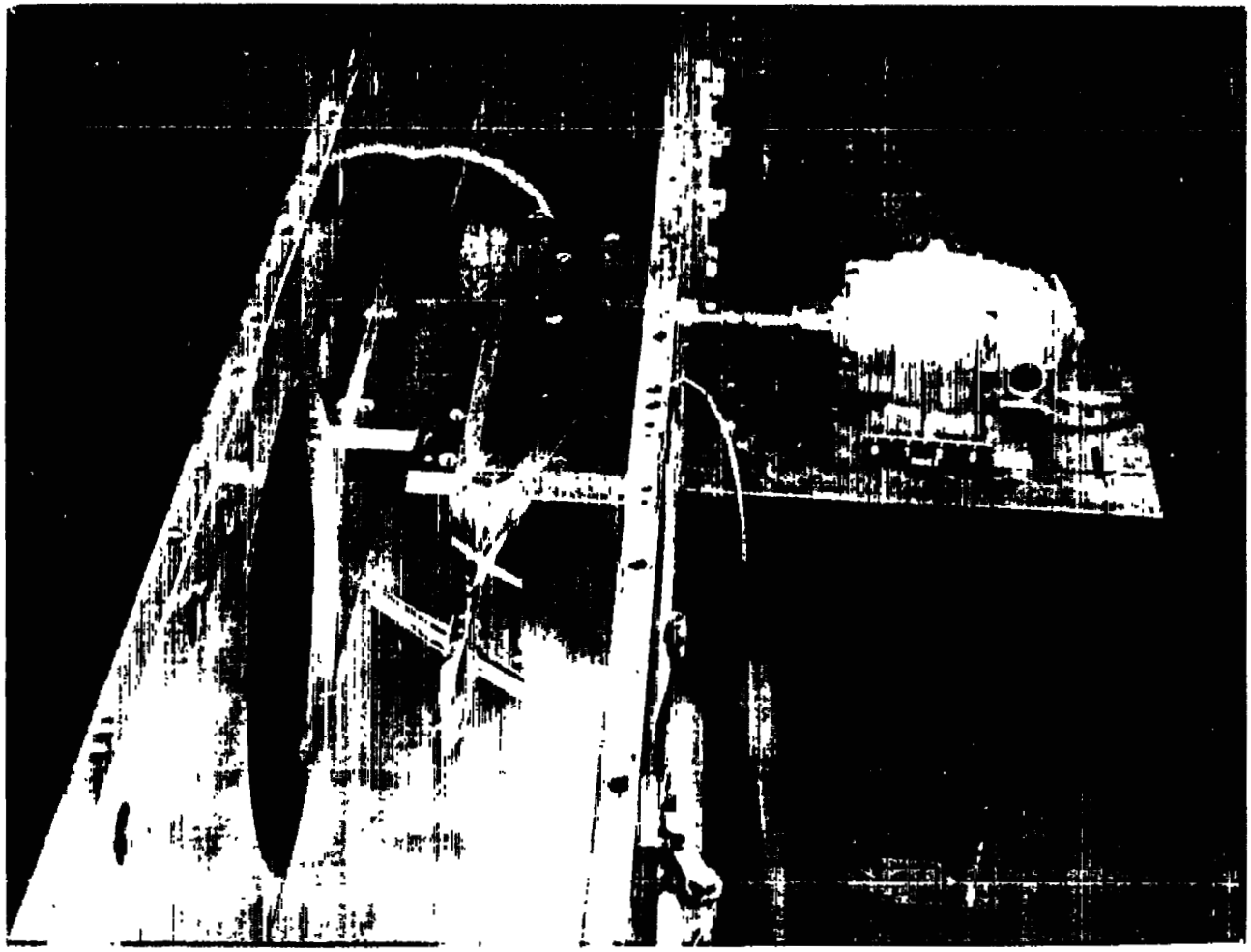

L-89408

(a) Setup in tunnel (top nozzle block removed).

Figure 2.- Photographs of the damping-in-roll test apparatus and the complete model.

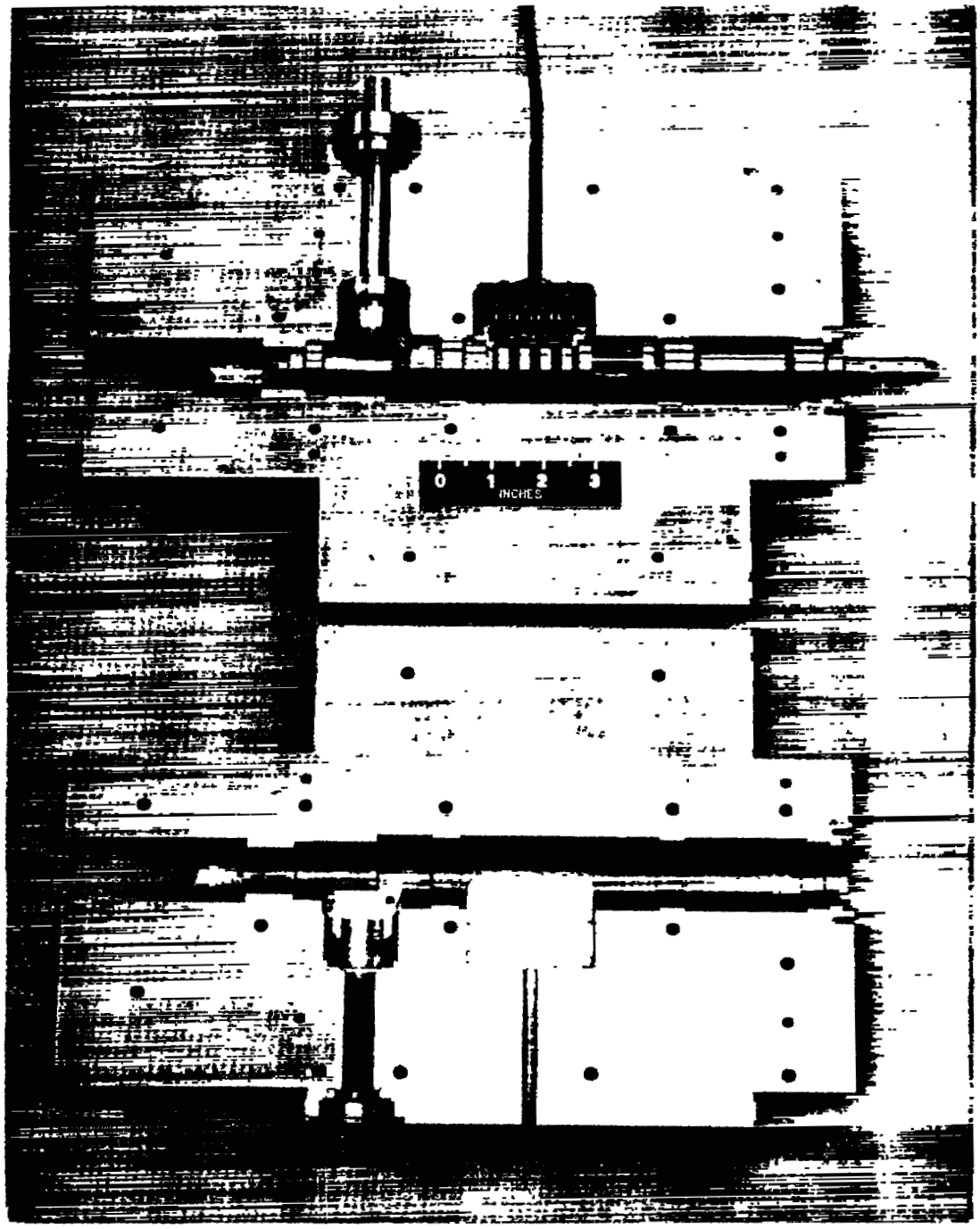

L-89409

(b) Interior of balance.

Figure 2.- Concluded.

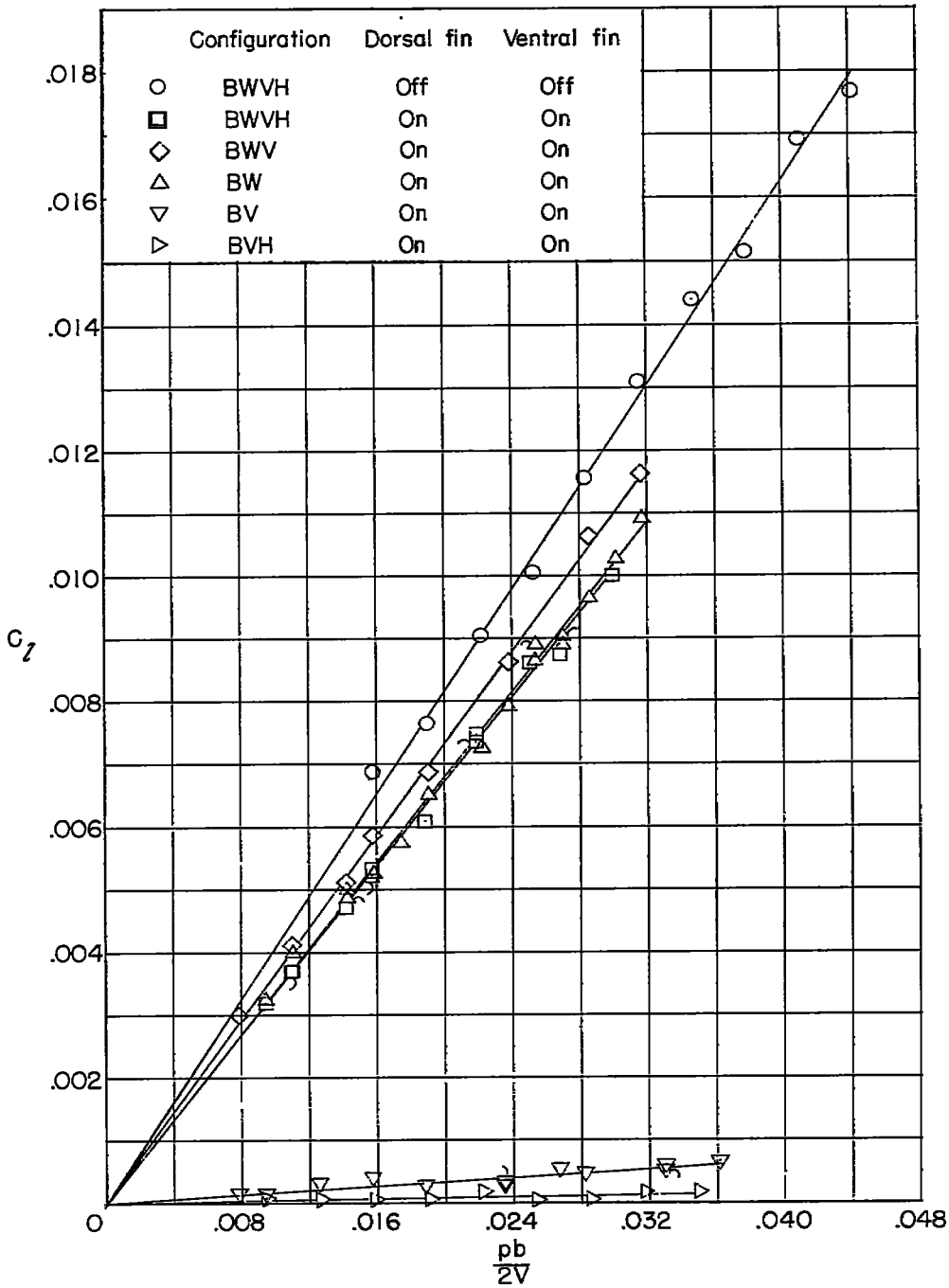

(a) M = 1.62.

Figure 3.- Variations of rolling-moment coefficient with wing-tip helix angle of the complete model and its components at zero angle of attack. Flagged symbols indicate check points.

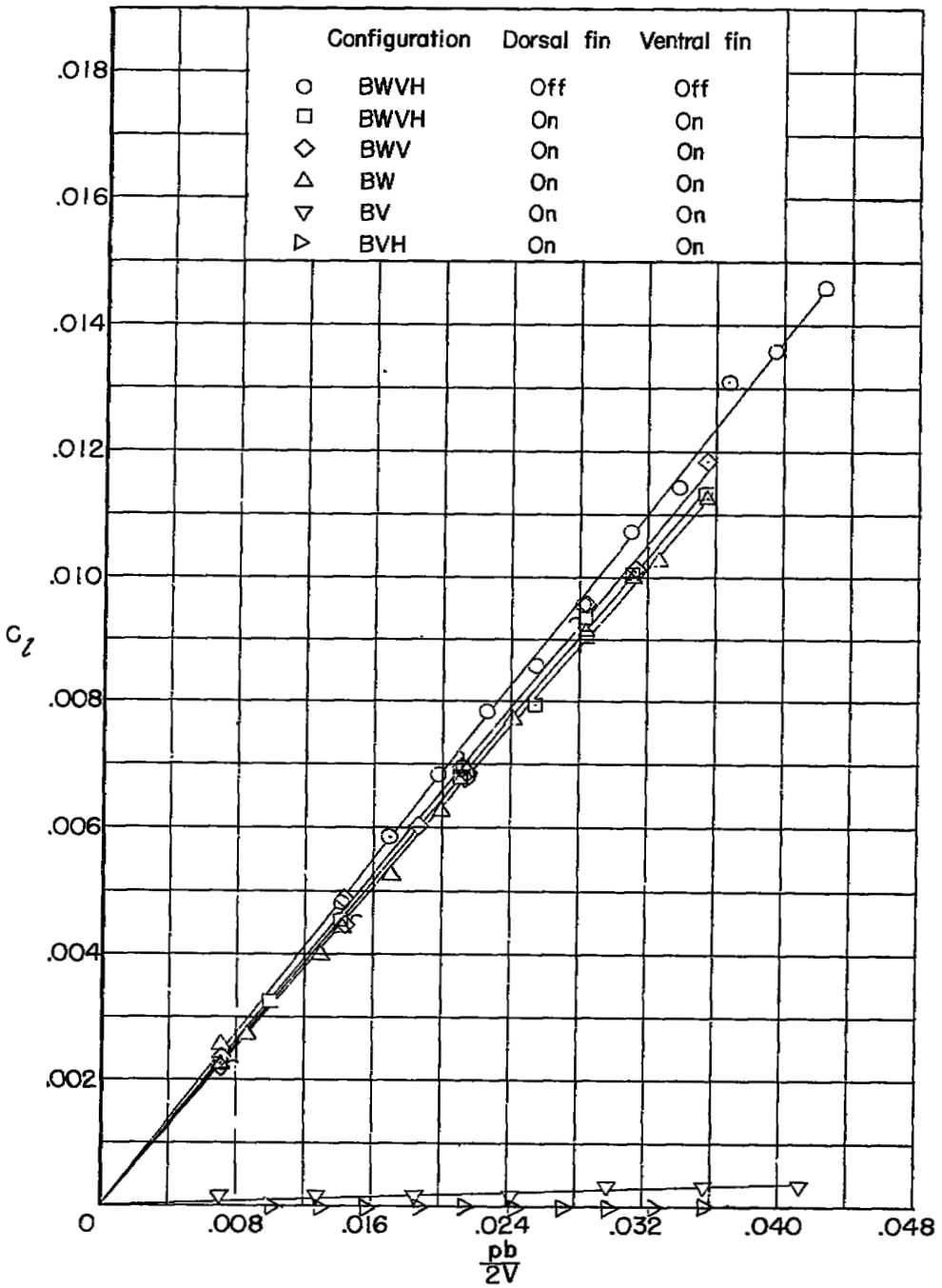

(b) M = 1.94.

Figure 3.- Continued.

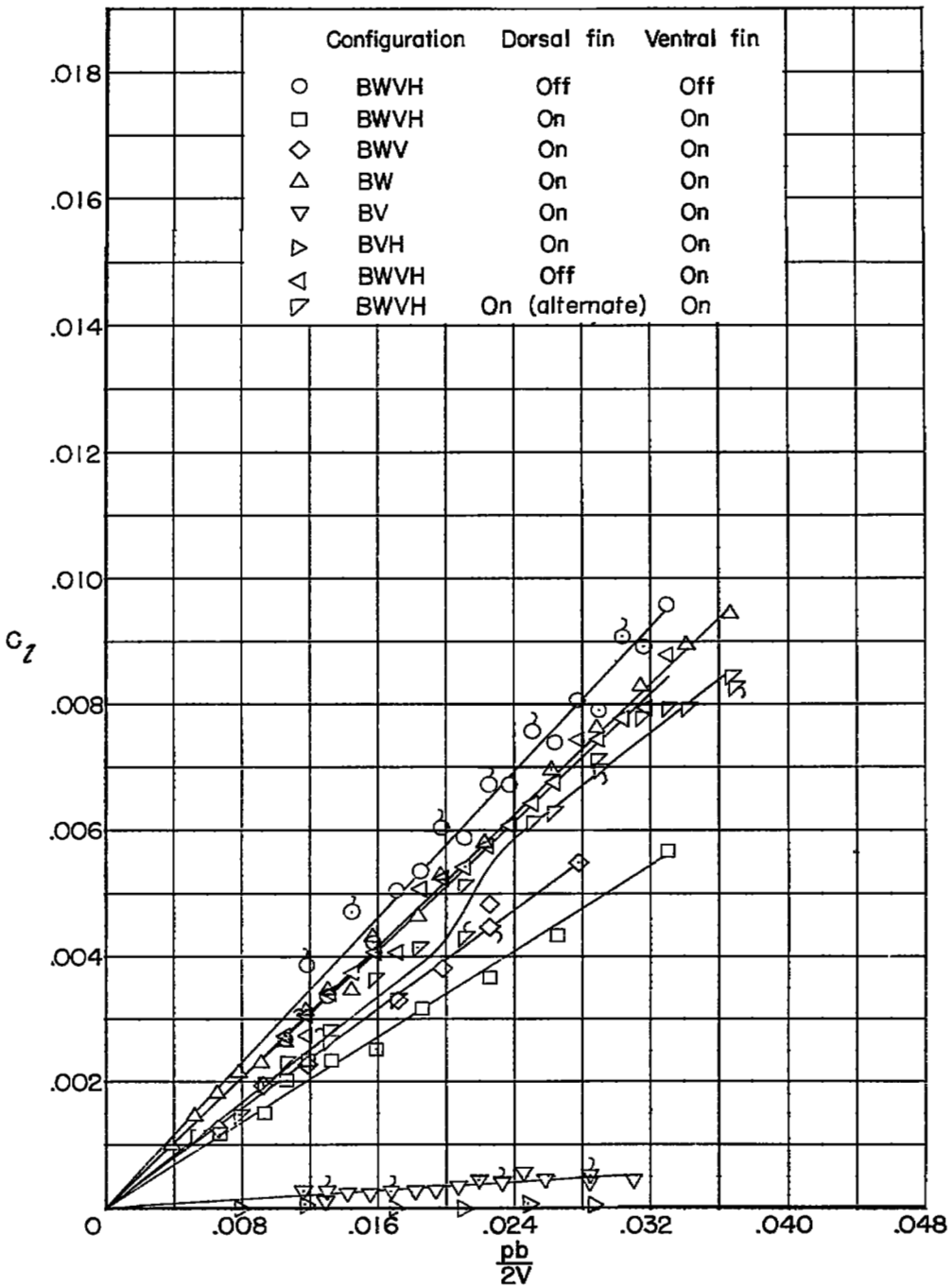

(c) M = 2.22.

Figure 3.- Continued.

[redacted]

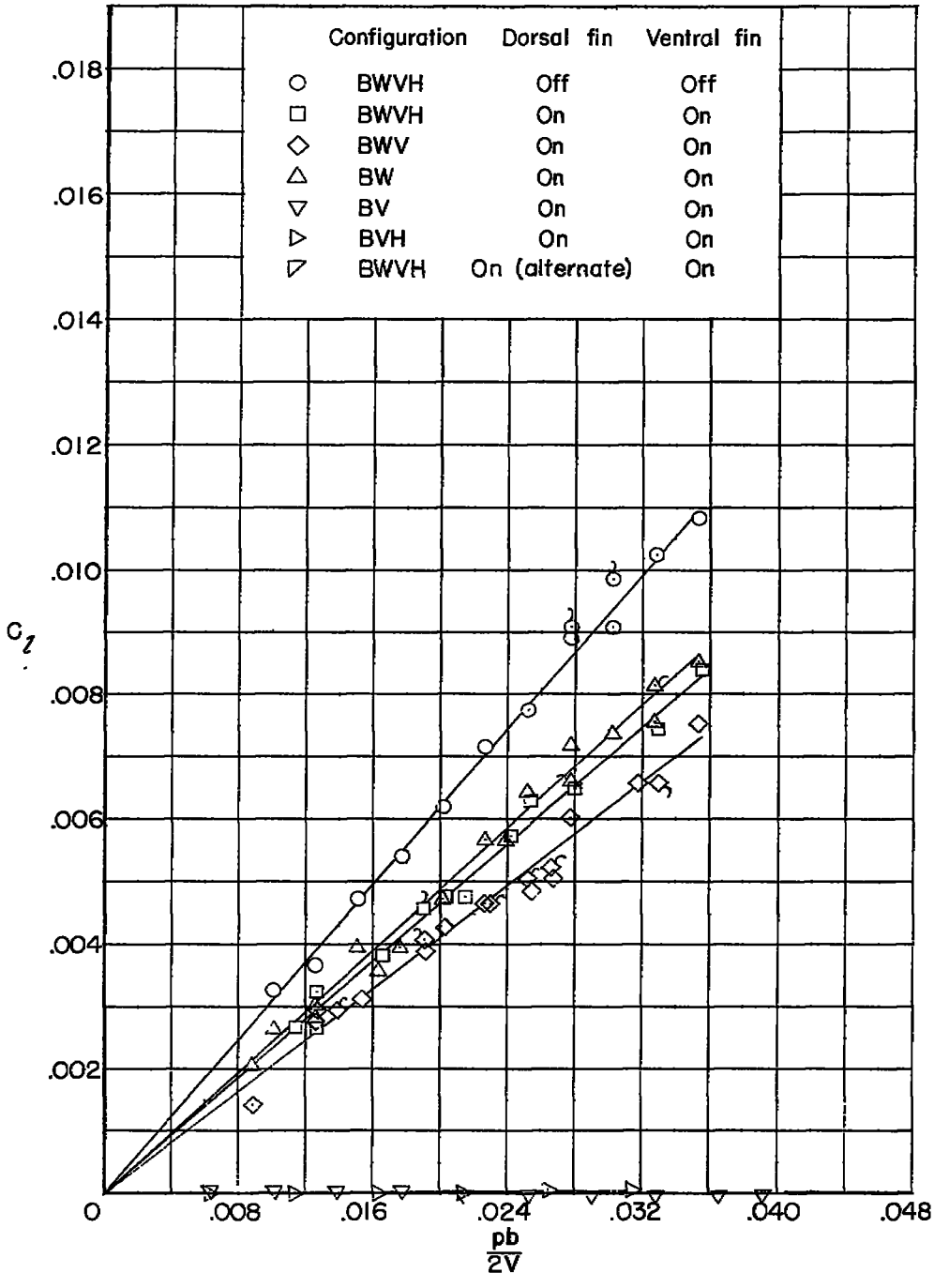

(d) M = 2.41.

Figure 3.- Continued.

[redacted]

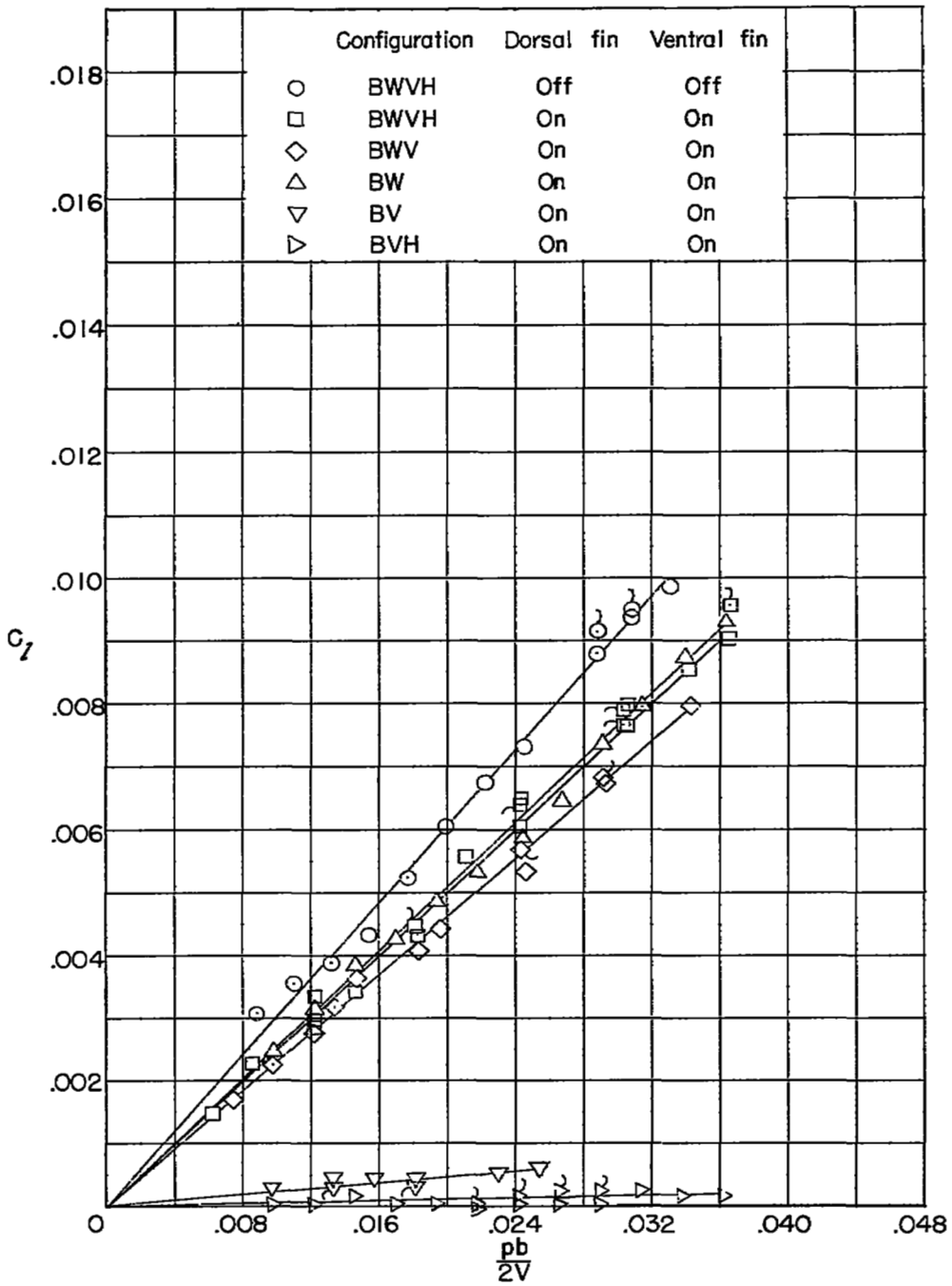

(e) M = 2.62.

Figure 3.- Concluded.

[redacted]

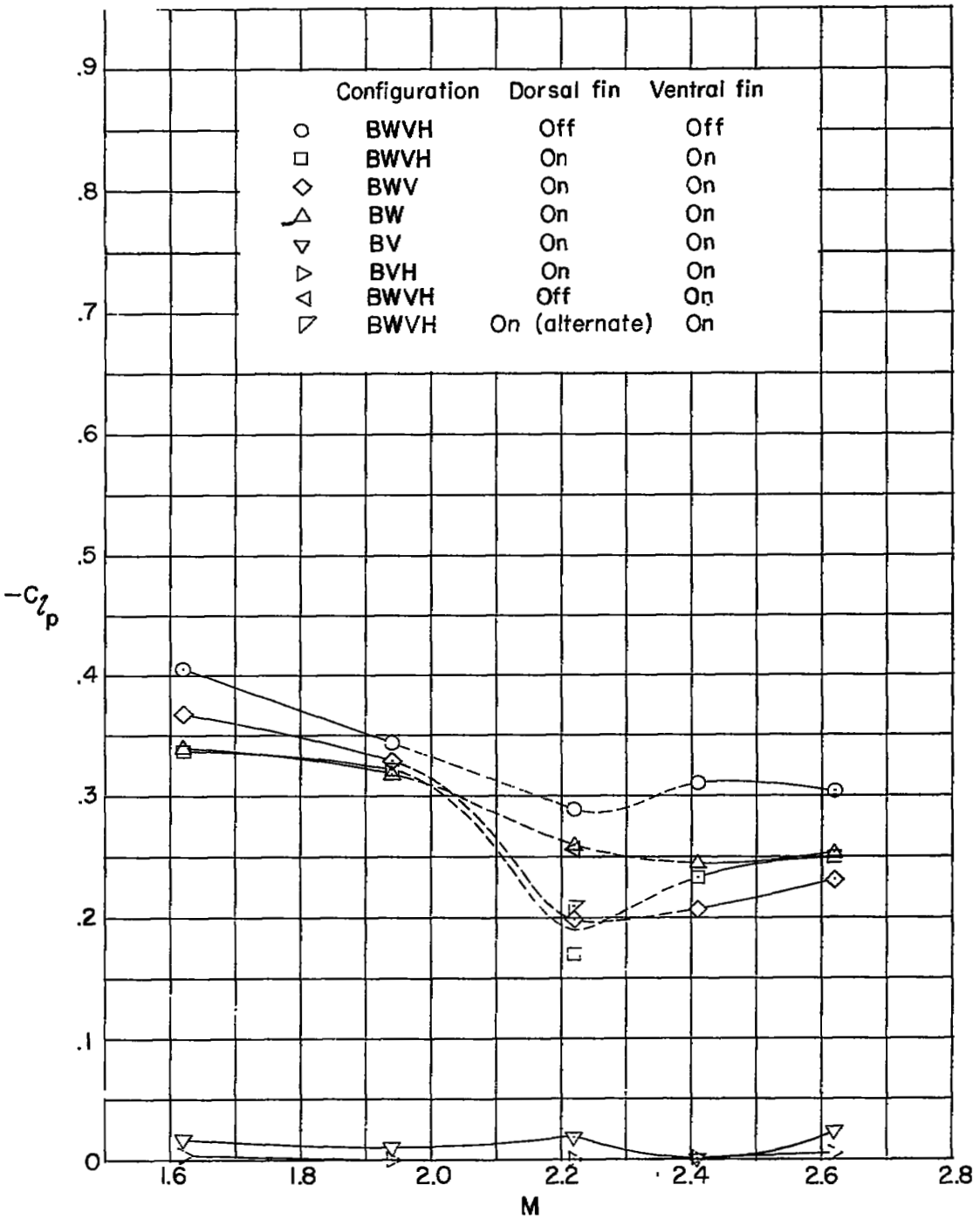

Figure 4.- Variations with Mach number of the damping in roll of the complete model and its components at zero angle of attack. Dashed portions of curves denote uncertain fairing.

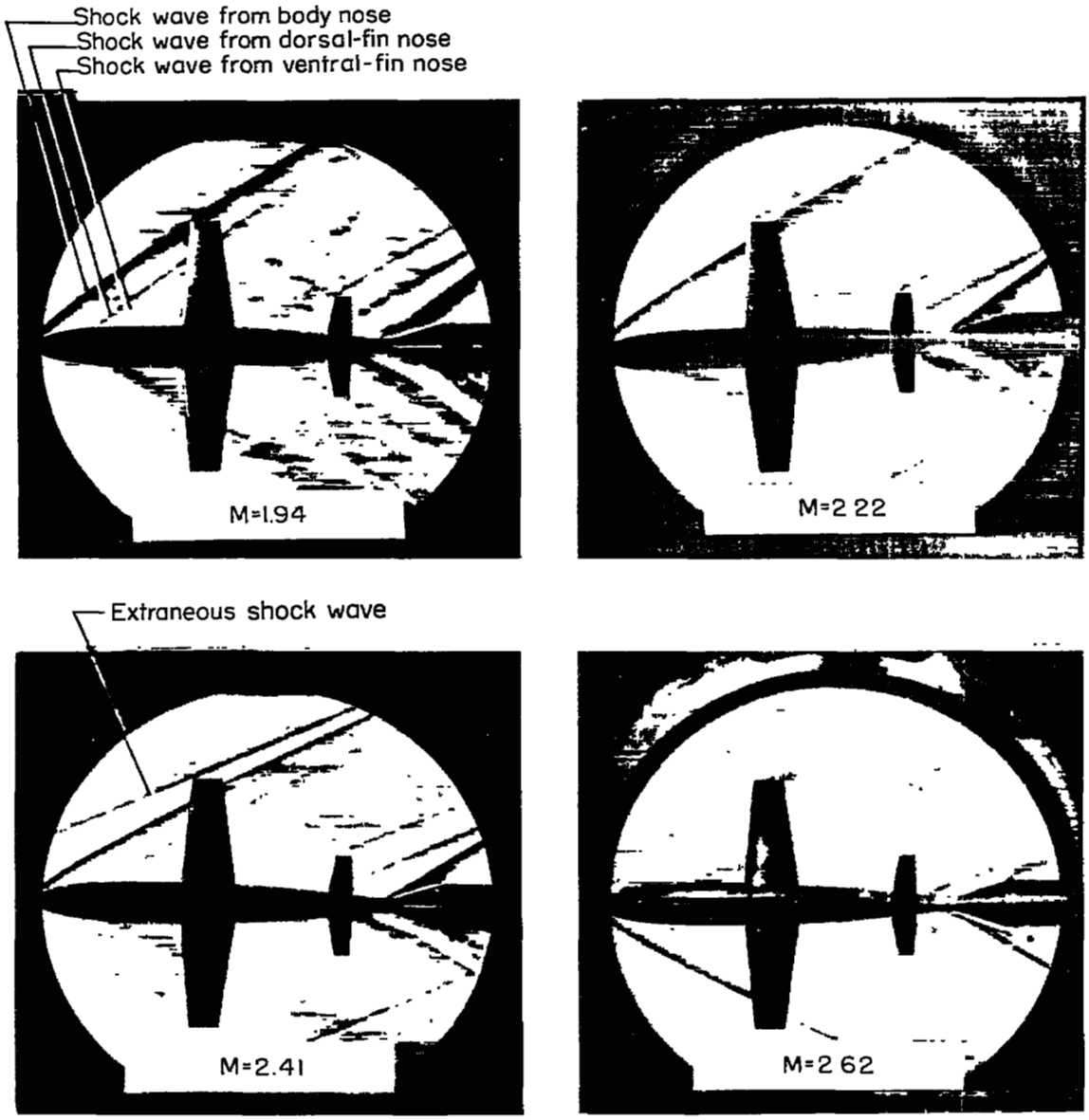

L-89391

Figure 5.- Schlieren photographs of the flow about the complete model at zero rolling velocity. $\alpha = 0^{\circ}$.

[redacted]

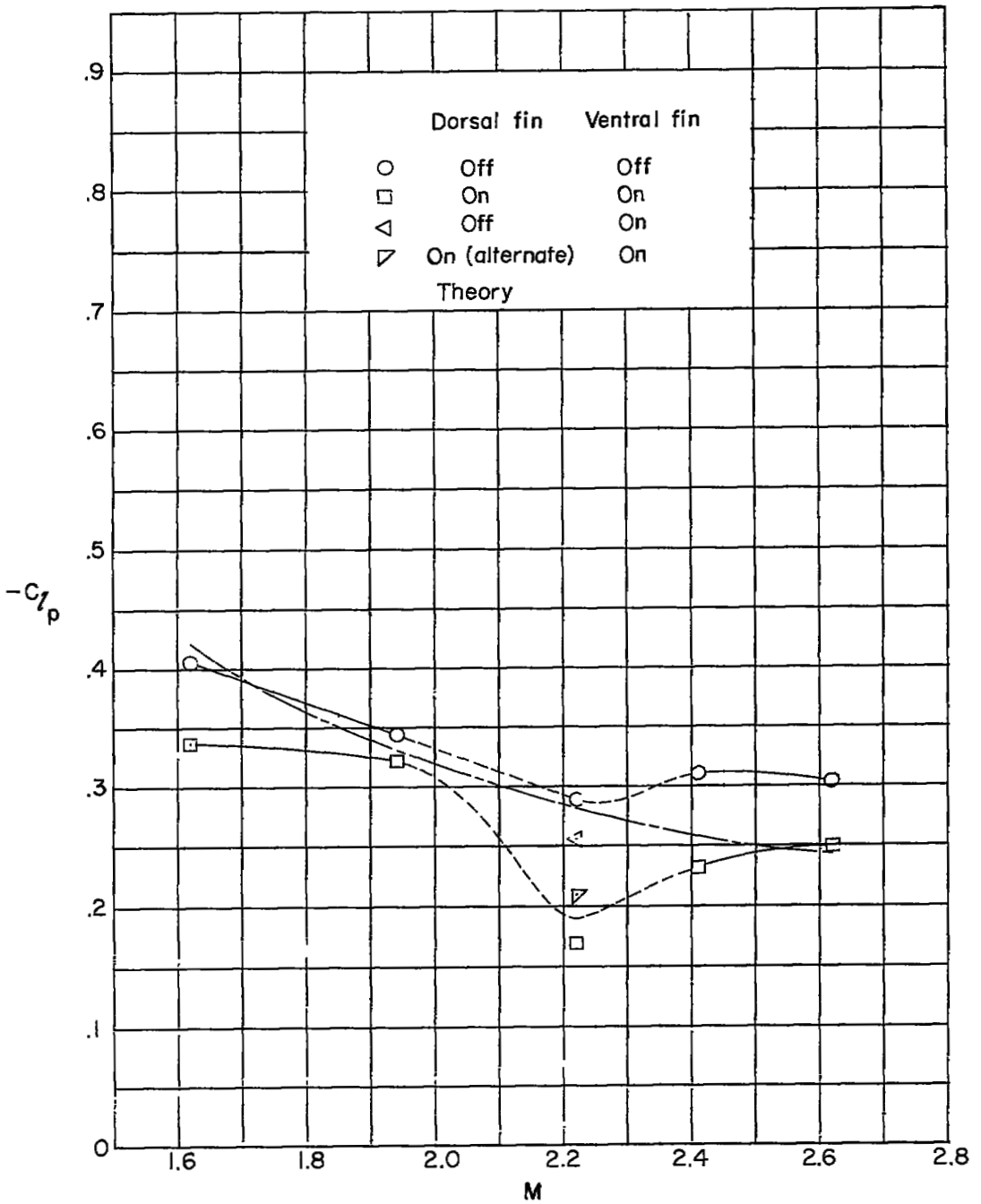

(a) BWVH.

Figure 6.- Variations with Mach number of the experimental and theoretical damping in roll at zero angle of attack. Dashed portions of experimental curves denote uncertain fairing.

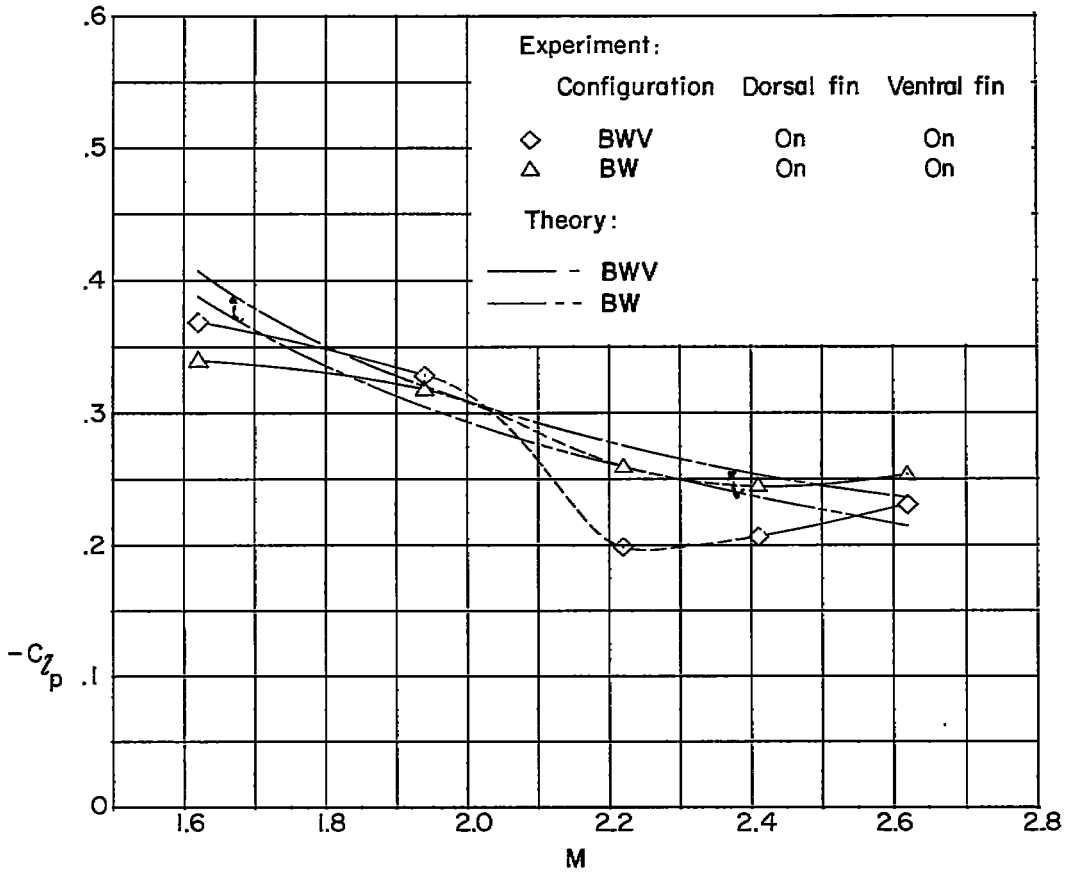

(b) BW and BWV.

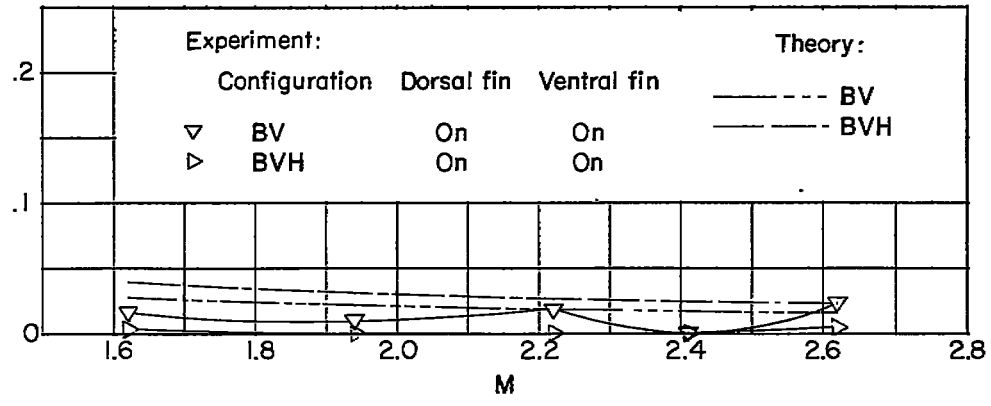

(c) BV and BVH.

Figure 6.- Concluded.

[redacted]

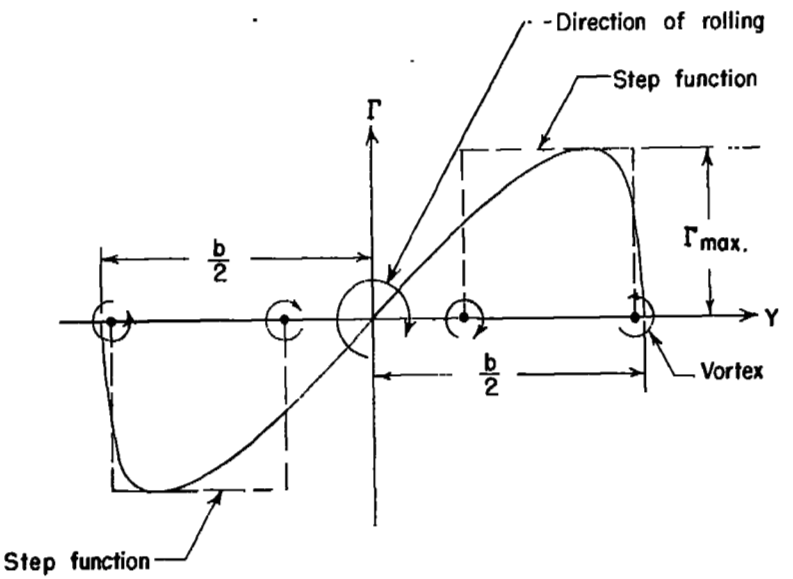

(a) Distribution of circulation along the wing span.

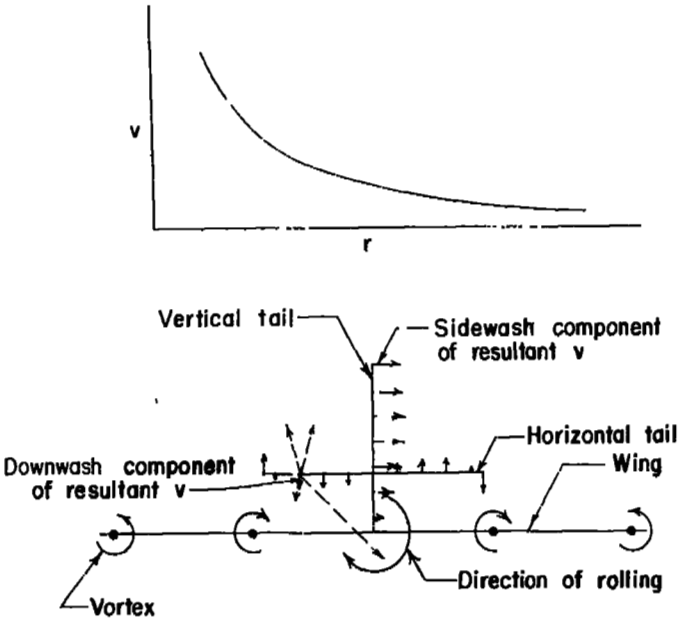

(b) Rear view of model, showing the wing trailing vortices and the velocities induced on the tail panels.

Figure 7.- Approximation of the wing flow field and its effects on the tail panels.